

Accepted Manuscript

Title: Efficient Pt electrocatalysts supported onto flavin mononucleotide–exfoliated pristine graphene for the methanol oxidation reaction

Author: <ce:author id="aut0005" author-id="S0013468616327360-58a4ee6fa749b6f386ed46accb6f71a9"> M. Ayán-Varela<ce:author id="aut0010" author-id="S0013468616327360-0e2d9cfd315ef0e9b82405f4638c6312"> R. Ruiz-Rosas<ce:author id="aut0015" author-id="S0013468616327360-4f3568c072258e8e85f780e378e9cf5d"> S. Villar-Rodil<ce:author id="aut0020" author-id="S0013468616327360-3ab87ca6e1f59d6f1bfece4cecfad804"> J.I. Paredes<ce:author id="aut0025" author-id="S0013468616327360-9cc7d3ed4bf15963b97b4c7fde90ae99"> D. Cazorla-Amorós<ce:author id="aut0030" author-id="S0013468616327360-3a17beb31fe0b703120fedc652b99929"> E. Morallón<ce:author id="aut0035" author-id="S0013468616327360-abcde6b0cfc5bacab0b460cba85c02ad"> A. Martínez-Alonso<ce:author id="aut0040" author-id="S0013468616327360-cfc5e8ac9414244ee8d01252d8b9a476"> J.M.D. Tascón

PII: S0013-4686(16)32736-0
DOI: <http://dx.doi.org/doi:10.1016/j.electacta.2016.12.177>
Reference: EA 28649

To appear in: *Electrochimica Acta*

Received date: 4-10-2016
Revised date: 13-12-2016
Accepted date: 27-12-2016

Please cite this article as: M.Ayán-Varela, R.Ruiz-Rosas, S.Villar-Rodil, J.I.Paredes, D.Cazorla-Amorós, E.Morallón, A.Martínez-Alonso, J.M.D.Tascón, Efficient Pt electrocatalysts supported onto flavin mononucleotide–exfoliated pristine graphene for the methanol oxidation reaction, *Electrochimica Acta* <http://dx.doi.org/10.1016/j.electacta.2016.12.177>

This is a PDF file of an unedited manuscript that has been accepted for publication. As a service to our customers we are providing this early version of the manuscript. The manuscript will undergo copyediting, typesetting, and review of the resulting proof before it is published in its final form. Please note that during the production process errors may be discovered which could affect the content, and all legal disclaimers that apply to the journal pertain.

**Efficient Pt electrocatalysts supported onto flavin mononucleotide–exfoliated
pristine graphene for the methanol oxidation reaction**

M. Ayán-Varela^{a,*}, R. Ruiz-Rosas^b, S. Villar-Rodil^a, J. I. Paredes^a, D. Cazorla-
Amorós^b, E. Morallón^b, A. Martínez-Alonso^a, J. M. D. Tascón^a

^aInstituto Nacional del Carbón, INCAR-CSIC, Apartado 73, 33080 Oviedo, Spain

^bInstituto Universitario de Materiales, Universidad de Alicante, 03690 San Vicente del
Raspeig, Alicante, Spain

* Corresponding author: Telephone: (+34) 985 11 90 90. Fax: (+34) 985 29 76 62. E-mail address: m.ayan@incar.csic.es (M. Ayán-Varela)

Abstract

Due to its large surface area, high electrical conductivity as well as mechanical and thermal stability, pristine graphene has the potential to be an excellent support for metal nanoparticles (NPs), but the scarce amount of intrinsic chemical groups/defects in its structure that could act as anchoring sites for the NPs hinders this type of use. Here, a simple strategy based on the stabilization of pristine graphene in aqueous dispersion with the assistance of a low amount of flavin mononucleotide (FMN) is shown to yield a material that combines high electrical conductivity and abundance of extrinsic anchoring sites, so that pristine graphene–metal (Pd and Pt) NP hybrids with good dispersion and metal loading can be obtained from FMN–stabilized graphene. The activity of these hybrids towards the methanol oxidation reaction (MOR) both in acidic and alkaline media is studied by cyclic voltammetry (CV) and their stability investigated by chronoamperometry. The pristine graphene–Pt NP hybrid prepared by this simple, eco–friendly protocol is demonstrated to outperform most previously reported pristine graphene– and reduced graphene oxide–metal NP hybrids as electrocatalyst for the MOR, both in terms of catalytic activity and stability, avoiding at the same time the use of harsh chemicals or complex synthetic routes.

Keywords: fuel cell, methanol oxidation reaction, electrocatalyst, graphene, biomolecule, metal nanoparticles

1. Introduction

Owing to the increasing demand of sustainable alternatives to the environmentally troublesome fossil fuels extensively used nowadays, direct methanol fuel cells (DMFCs) have attracted significant attention over the last years as an efficient portable power source for electronic devices [1,2]. This interest is due to the easy transport, storage and manipulation of liquid fuels, as well as to the high energy conversion efficiency and low operation temperature and pollutant emission associated to DMFCs [3,4]. On the other hand, DMFCs suffer from two remarkable disadvantages: (1) methanol crossover in the electrolyte membranes from the anode to the cathode and (2) sluggish kinetics of the methanol oxidation reaction (MOR) [5-7]. To address the

former issue, a lot of effort has been focused on the development of new proton and anion exchange membranes [8,9]. To mitigate the latter limitation, a common strategy involves the use of suitable electrocatalysts to overcome the activation barrier associated to the MOR. In this regard, it is well known that Pt is the most active metal electrocatalyst [10-12], but other metals (e.g., Pd, Ni, Co or Cu) and metal alloys are also explored because of their lower cost and better tolerance to poisoning by CO [13-16]. In addition to the electrocatalyst itself, proper selection of a good support material is a critical issue, due to its potential influence on the size, distribution and morphology of the metal component. For application in DMFCs, ideal supports must have a large surface area, high conductivity and should be able to anchor and stabilize ultrafine metal nanoparticles (NPs), avoiding their aggregation.

Carbon materials, such as carbon nanotubes [17], carbon black [18], ordered mesoporous carbon [19], carbon nanofibers [20] and graphene [21], have emerged over the last years as suitable supports for metal NPs towards fuel cell applications. In particular, graphene exhibits a unique two-dimensional honeycomb atomic structure with large surface area, structural, mechanical and thermal stability as well as high charge carrier mobility and electrical conductivity [22,23]. These attractive features make graphene an excellent support for metal NPs, with a potential to enhance their electrocatalytic activity. Currently, the most common route to synthesize metal and other NPs onto graphene materials as supports takes advantage of the peculiar characteristics of a well-known derivative of graphene, i.e. graphene oxide (GO). GO boasts good dispersibility in water and some organic solvents, which facilitates the deployment of wet colloidal NP preparation methods, and is also extensively decorated with oxygen functional groups, which serve as tight anchoring sites for the nucleation and growth of the NPs [21,24-25,26].

However, the use of GO-based or reduced graphene oxide (RGO)-based supports in electrocatalytic applications has also significant drawbacks. For instance, the presence of oxygen functional groups, which cannot be completely removed by the usual reduction approaches, degrades the electrical conductivity of the carbon lattice and compromises its stability under the harsh electrochemical conditions of fuel cells [27]. Therefore, finding alternative graphene materials that can escape the limitations of GO but exhibit at the same time its main attractions would be highly desirable. Pristine graphene flakes and sheets are in principle an obvious option in this regard, because their oxide-free nature endows them with high electrical conductivity and

chemical/electrochemical stability. Indeed, a few recent studies have focused on metal NP-pristine graphene systems as electrocatalysts for alcohol fuel cells [28-33]. Such studies relied either on graphene layers synthesized by chemical vapor deposition (CVD) [28,31-33] or on flakes obtained by direct, ultrasound-assisted exfoliation of graphite powder in organic solvents, such as *N*-methyl-2-pyrrolidone (NMP) [29,30]. Nevertheless, the use of these specific types of pristine graphene is not without its disadvantages. For example, the synthesis of CVD graphene is a relatively complex process that requires high temperatures, whereas NMP is a high boiling point and non-innocuous solvent that encumbers further processing of the exfoliated graphene flakes (in this regard, production/processing in water would be clearly preferable). More generally, the absence (or very low density) of chemical groups and defects in pristine graphene materials makes their uniform decoration with firmly anchored NPs harder to attain. Thus, the deployment of simpler and safer methodologies towards the production of efficient pristine graphene–metal NP electrocatalysts for MOR is still in great demand.

A solution to the mentioned limitations of pristine graphene-supported electrocatalysts could be based on the use of certain amphiphilic molecules with the ability to strongly adsorb onto graphene and play a dual role: (1) they would act as colloidal stabilizers to afford the production and processing of pristine graphene flakes in aqueous medium and (2) they would serve as anchoring sites to allow extensive and uniform decoration of the flakes with metal NPs. In this respect, we have very recently demonstrated the utility of flavin mononucleotide (FMN), an innocuous and safe derivative of vitamin B₂, as an exceedingly efficient dispersant of pristine graphene flakes in water [34]. Significantly, very low fractions of FMN (FMN/graphene mass ratios down to 0.04) are able to colloidally stabilize high graphene concentrations (up to ~50 mg mL⁻¹), and the amphiphile is strongly adsorbed onto the graphene surface via π - π interactions, thus avoiding any significant structural alteration of the carbon lattice. As a result, FMN-based graphene films were shown to exhibit very high electrical conductivity. In addition, the adsorbed FMN molecules served as efficient extrinsic anchoring sites for the nucleation and growth of metal NPs on the graphene flakes. All these results suggest that FMN-based metal NP-pristine graphene hybrids could possess a strong potential as high performance electrocatalysts for MOR, but studies along this line have not yet been undertaken. Hence, in the present work we have prepared Pt and Pd NPs onto FMN-stabilized graphene flakes and investigated their use as

electrocatalysts for MOR. The results indicate that these hybrids exhibit improved electrocatalytic activity in relation to many other graphene-based systems, and therefore constitute a highly competitive option for use in DMFCs as a result of, e.g., their simplicity of preparation or use of completely innocuous reagents (FMN).

2. Experimental section

Unless otherwise specified, all the chemicals and starting materials used in this work were supplied by Sigma–Aldrich Chemistry.

2.1. Preparation of FMN–stabilized pristine graphene and graphene-metal NP hybrids

A schematic of the production protocol of the pristine graphene-metal NP hybrids is given in Fig. 1. First of all, dispersions of graphene stabilized by FMN were prepared as described elsewhere [34]. Briefly, a mixture of natural graphite powder and FMN at a concentration of 30 mg mL⁻¹ and 1 mg mL⁻¹ in Milli-Q water, respectively, was sonicated during 5 hours in an ultrasonic bath cleaner (JP Selecta Ultrasons system, 40 kHz) at a power of 20 W L⁻¹. The obtained dispersion was centrifuged at 2300 rpm during 20 min (Eppendorf 5424 microcentrifuge) to eliminate the non–exfoliated material from the dispersion. The top ~75% of the resulting supernatant was collected as the FMN-graphene dispersion. To ensure the removal of free, non-adsorbed FMN, the dispersion was subjected to purification consisting of two cycles of sedimentation (14600 rpm, 20 min) and redispersion in Milli-Q water. The concentration of the resulting dispersion was calculated by measuring its UV-vis absorbance at a wavelength of 660 nm and applying the Lambert-Beer law [34].

The graphene-metal NP hybrids were prepared as follows. In the case of the graphene–Pt NP hybrid, a dispersion of FMN-graphene (9 mL, ~0.18 mg mL⁻¹) was heated in a sealed tube at 85 °C under magnetic stirring, and then 1 mL of K₂PtCl₄ (1.1 mM) aqueous solution was added. The reaction mixture was allowed to react during 2 h at such a temperature and then cooled down to ambient temperature. To eliminate the unreacted salt, this dispersion was completely precipitated (14600 rpm, 20 min) and redispersed in milli-Q water. Then, 20 µL of 1.5 M NaBH₄ was added and left to react undisturbed at room temperature for 45 min. For the synthesis of the graphene–Pd NP

hybrids, two protocols were used. The first protocol involved the use of ethanol as solvent and reductant. A solution of FMN-stabilized graphene (0.1 mg mL^{-1}) and PdCl_2 (0.17 mM) in ethanol-water mixture (1:1) was heated at $60 \text{ }^\circ\text{C}$ with magnetic stirring during 90 min and then allowed to cool down to ambient temperature. In the second protocol, $300 \text{ }\mu\text{L}$ of 5.6 mM aqueous PdCl_2 solution and $100 \text{ }\mu\text{L}$ of 1.2 M NaBH_4 were added to a sealed tube which contained a dispersion of FMN-stabilized graphene (9.7 mL , 0.1 mg mL^{-1}) at $70 \text{ }^\circ\text{C}$ with magnetic stirring, and then the mixture was allowed to react during 12 h. In what follows, the graphene-Pd NP hybrids prepared with ethanol and NaBH_4 as reductants are designated as graphene-Pd NP(1) and graphene-Pd NP(2), respectively. In all cases, the dispersions were purified by two cycles of sedimentation and resuspension in milli-Q water to obtain the final graphene-metal NP hybrid dispersions.

2.2. Characterization

The FMN-stabilized graphene dispersion was characterized spectroscopically by UV-vis absorption spectroscopy, Raman spectroscopy, and X-ray photoelectron spectroscopy (XPS), and microscopically by atomic force microscopy (AFM) and transmission electron microscopy (TEM). The pristine graphene-metal NP hybrids were characterized by TEM, XPS and inductively coupled plasma-mass spectrometry (ICP-MS). UV-vis spectra were recorded on a double-beam Helios α spectrophotometer, from Thermo Spectronic. Raman spectra were recorded with a laser excitation wavelength of 532 nm on a Jobin-Yvon LabRam apparatus. XPS was accomplished with a SPECS apparatus working at a pressure of 10^{-7} Pa and using a monochromatic $\text{Al K}\alpha$ X-ray source (100 W). Samples for XPS were prepared by casting the corresponding dispersion drop-wise onto a pre-heated ($50\text{--}60 \text{ }^\circ\text{C}$) flat metallic sample holder and allowing it to dry. AFM imaging was carried out with a Nanoscope IIIa Multimode instrument (Veeco) under ambient conditions. AFM measurements were performed in the tapping mode of operation using rectangular silicon cantilevers. To image individual graphene sheets, a small volume of diluted dispersion ($0.01\text{--}0.05 \text{ mg mL}^{-1}$) was drop-cast onto a preheated ($50\text{--}60 \text{ }^\circ\text{C}$) SiO_2 (300 nm)/Si substrate and allowed to dry. TEM imaging was performed on a JEOL 2000 EX-II instrument operated at 160 kV . A few microliters of aqueous sample suspension diluted with ethanol ($50:50 \text{ vol/vol } \%$) were drop-cast onto copper grids (200 mesh) covered with a carbon film and allowed to dry. ICP-MS analyses of the graphene-metal NP hybrids were performed with a 7500ce

(Agilent) instrument equipped with an octopole collision/reaction cell to destroy interfering ions. Prior to analysis, the hybrids were subjected to microwave-assisted acid digestion.

2.3. Electrochemical measurements

The electrochemical characterization of the electrodes was carried out in an Autolab PGSTAT302 potentiostat (Metrohm, Netherlands) using a conventional three-electrode cell configuration. The working electrode consisted of glassy carbon electrodes (GCEs) modified with the graphene–metal NP hybrids, while a platinum wire was used as the counter electrode. Ag/AgCl/3M KCl electrode was employed as the reference electrode in measurements using acid electrolyte, while a saturated calomel electrode (SCE) was used for measurements in basic electrolyte. All the potentials reported in this work were referred to that of the Reversible Hydrogen Electrode (RHE). Modified GCEs were prepared as follows. A GCE with a geometric area of 0.07 cm² was carefully polished with fine emery paper from big to small grain size and then ultrasonically cleaned in milli-Q water. The graphene–Pt or Pd NP hybrid film was prepared by drop-casting a certain volume of the corresponding aqueous graphene–metal NP dispersion of known concentration on the GCE surface to achieve a final hybrid content of ~10 µg, and then evaporating the solvent under an infrared heating lamp. The concentration of the hybrids was calculated taking into account both the concentration of graphene, extracted from UV-vis absorption measurements, and the metal loading of the hybrids, measured by ICP-MS [34Error! Bookmark not defined.]. Finally, to provide the graphene–metal NP hybrid film with better adhesion to the GCE surface, 2.9 µL of a 0.2 wt.% Nafion ® solution in ethanol (prepared from 5% wt. Nafion ® solution) was drop-cast on top of it.

The electrochemical behavior of the graphene–metal NP hybrids was studied by cyclic voltammetry in 0.5 M H₂SO₄ and in 0.1 M KOH. Cyclic voltamograms (CVs) were recorded using a scan rate of 50 mV s⁻¹ at room temperature. Nitrogen was bubbled into the solution to remove oxygen from the electrolyte for at least 20 min prior to the measurements as well as throughout the measurements. The electrochemically active surface area (ECSA) of Pt and Pd from the graphene–metal NP hybrids was determined from the CVs recorded in potassium hydroxide solution using the following equation:

$$\text{ECSA (m}^2 \text{ g}^{-1}\text{)} = Q \cdot m_{\text{NP}}^{-1} \cdot q_H^0 \quad (1)$$

Where Q is the electrical charge (C) after subtraction of the double layer measured from the integration of the voltammetric curve between 0.1 V and 0.45 V in the case of the Pt catalyst and between 0.45 V and 0.85 V in the case of both Pd catalysts; m_{NP} (g) is the loading of Pt or Pd in the graphene–metal NP hybrids; and q_H^0 (C m⁻²) is the charge for a monolayer of one electron adsorption-desorption processes on Pt and two electron reduction process in Pd, which are equal to 2.1 and 4.2 C m⁻², respectively [35,36].

In order to evaluate the electrochemical activity of the graphene–metal NP hybrids towards the methanol oxidation reaction (MOR), CVs at 50 mV s⁻¹ were recorded using the same previously described equipment in solutions of 0.5 M H₂SO₄ and 0.1 M KOH, containing 0.5 M CH₃OH (99.8% Purity, Merck). Several activation scans were performed until steady state CVs were attained. Chronoamperometric experiments in 0.1 M KOH and 1 M CH₃OH were obtained under an applied potential of 0.8 V in order to study the stability of the hybrids in alkaline conditions. The tests lasted for 30 minutes, with the current being recorded during this time.

3. Results and discussion

3.1. Synthesis and characterization of the FMN-graphene support and graphene–metal NP hybrids

Bath sonication of graphite powder in aqueous FMN solution followed by mild centrifugation and purification (see Experimental Section for details) yielded a black colored FMN-graphene aqueous dispersion (Fig. 2A) indicative of successful exfoliation, which displayed long-term colloidal stability. The UV-vis absorption spectrum of such a dispersion was that expected for pristine graphene (Fig. 2B), showing a maximum at a wavelength of 272 nm, which is attributed to $\pi \rightarrow \pi^*$ transitions in extended conjugated carbon structures. No bands indicative of the presence of FMN were found, which means that the purification step reduced the amount of FMN to a very low level (compared with graphene). TEM and AFM images (Figs. 2C and D, respectively) of the FMN–exfoliated graphene flakes revealed that the material was successfully exfoliated into thin platelets. The graphene nanosheets exhibited lateral sizes around 100 to 500 nm, with a thickness mostly (75% of the

flakes) between 1 to 5 monolayers [34]. The Raman spectrum of the exfoliated material was typical of graphitic materials with high structural order (Fig. 2E). Indeed, the first-order spectrum was dominated by the G band (1582 cm^{-1}), which is the only band present in crystalline graphite, while the D (1348 cm^{-1}) and D' (1620 cm^{-1}) bands, which are related to the presence of structural disorder [37-39], displayed relatively low intensities. The ratio of the intensities of D and G bands, I_D/I_G , which is indicative of the degree of structural disorder in graphite/graphene structures, was ~ 0.17 for the FMN-exfoliated material, which was a value similar to or lower than those reported in the literature for other high quality pristine graphene sheets exfoliated with the aid of surfactants [39-45]. The high resolution C1s XPS spectrum of the exfoliated sample (Fig. 2F) was typical of pristine graphitic materials. The mass ratio of FMN relative to graphene (~ 0.04) was calculated from the relative amounts of phosphorous and carbon detected in the survey XPS spectrum (not shown) [34]. Such a ratio was one order of magnitude lower than those reported in the literature for other efficient surfactants for the colloidal dispersion of graphene in aqueous media [40-47], which is clearly an advantage given that the presence of surfactants or other stabilizing agents can affect negatively the electrical and catalytic properties of the nanosheets [48-51]. Indeed, the conductivity of the FMN-exfoliated graphene films ($52\ 000\ \text{S m}^{-1}$)[34] was much higher than that of other as-prepared graphene films obtained from surfactant-stabilized dispersions in water.

Pristine graphene-metal NP hybrids were prepared by mixing FMN-exfoliated graphene dispersions with appropriate metal precursor salts followed by reduction with a proper reducing agent (see Experimental Section for details). TEM images confirmed the decoration of the graphene flakes with NPs (Figs. 3A-D). The fact that no stand-alone NPs (i. e., physically separated from the graphene flakes) were detected implies that the NPs grew exclusively on the nanosheets, which suggests that the NPs were efficiently anchored onto the graphene support. The NPs were well dispersed, without detection of large aggregates. This implies that the otherwise inert basal plane of pristine graphene was rendered efficient for NP anchoring by the presence of strongly adsorbed FMN molecules. Thus, the simple preparation method of pristine graphene facilitated by FMN described here provides efficient and abundant anchoring sites for growing metal NPs on the flakes without the need of harsh chemicals or sophisticated

synthesis protocols involved in the preparation of other graphene-based catalysts, e. g., those using GO and RGO. The amount of metal precursor salts was optimized in every case to obtain a significant but not too high density of metal NPs on the surface. Lower concentrations of precursor salts than the ones finally chosen (see Experimental Section) yielded correspondingly lower numbers of NPs, while significantly higher starting concentrations led to very high densities of NPs on the surface, which was even detrimental to the colloidal stability of the nanosheets.

Figs. 3E and F show NP size distributions for graphene-Pt NP and graphene-Pd NP(1) hybrids, respectively. The average NP size is 4 ± 1 nm for the graphene-Pt NP hybrid, 13 ± 4 nm for the graphene-Pd NP(1) hybrid, and 9 ± 3 nm the graphene-Pd NP(2) hybrid. XPS analyses confirmed that Pt and Pd were in metallic form, as intended. Indeed, the high resolution Pt 4f core level spectrum of the graphene-Pt NP hybrid (Fig. 3G) and the Pd 3d spectrum of graphene-Pd NP(1) (Fig 3H) revealed the presence of Pt⁰ and Pd⁰, respectively, but not of metals in oxidized form. ICP-MS analysis allowed quantification of the metal content in the hybrids: 8 wt% Pt (graphene-Pt NP hybrid), 21 wt% Pd (graphene-Pd NP(1) hybrid,) and 17 wt% Pd (graphene-Pd NP(2) hybrid.). It is noteworthy that the increased concentrations of precursor salts tested during the optimization of the amount of metal precursor salt did not lead to larger metal NP sizes, but rather to a higher density of NPs, as mentioned above. In fact, no agglomeration of the metal NPs was observed on the surface, even at the highest precursor concentrations tested, which points to the existence of a strong interaction between the NPs and the graphene nanosheets. We believe that such interaction comes from both the strong adsorption of FMN onto the graphene surface via π - π interactions and the effective interaction of the metal with the phosphate groups and/or the hydroxyl groups in the ribitol moieties. Thus, owing to the strong adsorption of FMN, efficient and homogeneous anchoring sites are generated for the growth of metal NPs. Thus, while pristine graphene displays an inert surface with no functional groups or defects that could act as anchoring sites, FMN-stabilized graphene offers an abundance of anchoring sites. In comparison with GO or RGO, FMN-stabilized graphene could offer higher uniformity both in the spatial distribution and in the chemical nature of the anchoring sites, which would be expected to result in a better dispersion of the NPs on the nanosheets.

3.2. Electrocatalytic activity of the graphene–metal NP hybrids towards MOR

To investigate the potential application of the present graphene–metal NP hybrid materials towards MOR, the electrochemical behavior, stability and Pt and Pd ECSA were measured from CVs performed in a solution of 0.5 M H₂SO₄ (scan rate: 50 mV s⁻¹). The steady-state voltammograms of the graphene–Pt NP, graphene–Pd NP(1) and graphene–Pd NP(2) samples are shown in **Fig. 4**. Firstly, CVs were recorded between 0.1 and 1.2 V, and then the upper potential limit was opened 0.2 V up to 1.4 V in steps of 0.1 V. In all cases, clear hydrogen and anion adsorption–desorption peaks could be observed in the potential range of 0.1–0.45 V. For graphene–Pt NP and graphene–Pd NP(1) hybrids, the reduction peak associated to platinum and palladium oxide increased when the potential range was opened (**Fig. 4A and B**), while the hydrogen adsorption–desorption peaks became slightly more defined. However, the stability of the graphene–Pd NP(2) hybrid was lower (**Fig. 4C**), and the redox processes associated to hydrogen adsorption–desorption decreased when the potential was increased. The electrochemical behavior of these hybrids was also assessed in alkaline electrolyte, (**Fig. 4D**). All the obtained voltammetric profiles were consistent with those of polycrystalline Pt and Pd.

The ECSA of these hybrids was determined from the voltammograms recorded in alkaline media (Fig. 4D) and compiled in Table 1. The ECSA of the graphene–Pt NP hybrid was evaluated between 0.1 V and 0.45 V, being 49.2 m² g⁻¹, while in the case of Pd-supported electrocatalysts, the reduction of palladium oxide has been used. In these cases, the ECSA values obtained for the graphene–Pd NP(1) and (2) hybrids were 24.6 and 26.3 m² g⁻¹, respectively. The larger ECSA value of the graphene–Pt NP hybrid might be related to its smaller particle size, as seen by TEM (**Fig. 3E**). However, no clear relationship is found between ECSA and particle size in the case of the graphene–Pd NP hybrids. We have estimated the geometrical surface area (GSA, m² g⁻¹) of Pt and Pd in these samples, by assuming that the metal NPs were spherical and calculating the average surface with the diameter measured by TEM (Table 1). The electrocatalytic utilization of metal is higher for the Pt (79%) and Pd NP(1) (66%) hybrids, being lower for the Pd NP(2) hybrid (40%). The ECSA values of these graphene–metal NP hybrids were in the range of those reported in the literature for Pt– and Pd–based catalysts supported on pristine graphene [28-32] or graphene–related materials, such as RGO [52-61]. It is noteworthy that the simple preparation method described here yields

graphene–metal NP hybrids with acceptable ECSAs without the need of harsh chemicals or sophisticated synthesis protocols involved in the preparation of other graphene–based catalysts [62].

Fig. 5A shows the CV curve of methanol electro-oxidation in acid electrolyte for the graphene–Pt NP hybrid catalyst. The current shown in this CV was registered in the 0.1 V – 1.3 V potential range and given relative to the Pt mass loading. Table 1 compiles the current values and the forward to backward current ratio in acid ($I_F/I_B^{\text{H}_2\text{SO}_4}$) and alkaline (I_F/I_B^{KOH}) electrolyte for the hybrids prepared in this work. The values for these parameters as reported in other relevant work from the literature have been also provided for comparison purposes. For the acid electrolyte, the graphene–Pd NP hybrids showed much lower catalytic activity compared to that of the graphene–Pt NP hybrid (results not shown). In the case of the graphene–Pt NP hybrid, the onset potential for methanol oxidation was observed to be located at 0.40 V, and the oxidation forward and reverse peaks of methanol were located at 0.87 and 0.66 V, respectively. The graphene–Pt NP hybrid exhibited a forward peak current ($j_F^{\text{H}_2\text{SO}_4}$ on Table 1) of 1141 A g⁻¹, which is similar to the highest values that have been reported for RGO–Pt NP catalysts [52–54,58,63,64], and it was higher than those achieved using pristine graphene as support [31–33] and comparable to those achieved using bi- and tri-metallic NPs over pristine graphene [29]. The forward oxidation current to reverse current ratio (I_F/I_B on Table 1) describes the catalyst tolerance to CO-like intermediates that are formed on the surface of the catalyst during the forward CV sweep [10]. This ratio was around 1.00 for the pristine graphene–Pt NP hybrid in acidic medium, being lower than the value attained on RGO–based electrocatalysts, where the presence of surface oxygen functionalities promoted the complete oxidation of methanol to CO₂. However, the CO tolerance of the reported graphene–Pt NP catalyst was superior to that shown by other electrocatalysts prepared using pristine graphene as the carbon support [31–33], and similar to that seen for ultrafine Pt NPs on pristine graphene prepared by a supercritical CO₂ route [29].

The kinetics of MOR was more favorable in alkaline medium, which can render metals other than Pt (e. g., Pd) cost–effective as electrocatalysts [56]. Furthermore, the problems that traditionally hampered its applicability, such as carbonation of the electrolyte or the lack of high performance anion-exchange membranes have been already overcome [65]. Here, to explore the applicability of the pristine graphene–metal

NP hybrids in alkaline medium, their CVs were also measured in 0.5 M MeOH with 0.1 M KOH as shown in **Fig. 5B-D**. The onset potential for the graphene–Pt NP catalyst was 0.45 V, being lower than that shown by catalysts based on Pd NPs (0.57 V). The same differences were observed when the maximum of the forward oxidation current peak was considered (0.89 vs 0.80 V). The forward oxidation current of the pristine graphene–Pt NP hybrid was similar to the one recorded in acidic medium (Table 1), while as anticipated, the graphene–Pd NP hybrids displayed a much higher catalytic activity in alkaline medium than they did in acidic medium, with the best results being achieved for the graphene–Pd NP(2) sample (forward oxidation specific currents 154 and 201 A g⁻¹ for the graphene–Pd NP(1) and the graphene–Pd NP(2) hybrids, respectively). The catalytic activity obtained with the graphene–Pt NP hybrid was between five to seven times higher than those achieved with the graphene–Pd NP hybrids. Moreover, when the specific currents were normalized using the respective ECSA of each hybrid, the activity was seen to be enhanced in the case of the graphene–Pt NP hybrid (24.0 A m⁻² for the graphene–Pt NP hybrid vs 6.3 and 7.6 A m⁻² for the graphene–Pd NP(1) and the graphene–Pd NP(2) hybrids, respectively). It should be highlighted that the CO tolerance (as represented by the I_F/I_B parameter) was greatly improved in alkaline media, which is an already known feature that is based on the different MOR mechanisms [65,66]. Interestingly, the graphene–Pd NP(2) hybrid had a higher I_F/I_B ratio than the graphene–Pt NP hybrid (~4.9 vs 4.0, respectively; Table 1). Indeed, it has been demonstrated that Pd-containing electrocatalysts exhibit superior performance than that of Pt-based electrocatalysts in terms of poisoning resistance, which seems to be connected to the lower formation of CO-like species when Pd is used as the active phase [67].

To further verify the durability of these catalysts, potentiostatic chronoamperometry experiments were carried out in 0.1 M KOH, as shown in **Fig. 6**. As expected, a decay of the current density was found for all the catalysts due to formation of intermediate carbon-containing species during the oxidation of methanol. The most rapid initial decay was observed for the graphene–Pd NP(1) catalyst. In contrast with the I_F/I_B ratio previously reported, the lowest rate of decay was found for the Pt-based catalyst. Current retentions of 23, 5 and 2 % were measured after 30 min for the graphene–Pt NP, graphene–Pd NP(1) and graphene–Pd NP(2) catalysts, respectively. The specific current retained by the graphene–Pt NP hybrid after 30 minutes was in most cases higher than or at least amongst the highest of those recorded for similar catalysts reported in the

literature [54,63,64]. However, it is important to note that most of the mentioned graphene–Pt NP catalytic stability tests were conducted in acidic media.

Thus, the performance of the prepared pristine graphene–Pt NP hybrid as electrocatalyst in the MOR was found to be superior to that of previous Pt catalysts that used pristine graphene supports, on account of its good CO tolerance and stability as well as higher catalytic activity.

4. Conclusions

The performance of pristine graphene–metal NP hybrids (prepared from FMN–stabilized aqueous colloidal graphene dispersions) as electrocatalysts for the MOR has been investigated both in acidic and in basic media. Amongst the different graphene–metal NP hybrids prepared in this work, a graphene–Pt NP hybrid was found to be a particularly attractive electrocatalyst for MOR in terms of catalytic activity, stability and CO tolerance. In fact, this graphene–Pt NP material outperformed most of Pt NP-based electrocatalysts reported in the literature using RGO or pristine graphene as a support. Overall, these electrochemical studies confirm that exfoliation of pristine graphene using FMN as stabilizer is a suitable method for accessing a metal NP support that can deliver enhanced catalytic performance to the final electrocatalyst. This simple, environmentally–friendly preparation method avoids the use of harsh chemicals or complex synthetic routes involved in the preparation of other graphene-supported catalysts.

Acknowledgements

Financial support from the Spanish Ministerio de Economía y Competitividad (MINECO) and the European Regional Development Fund (FEDER) through projects MAT2015-69844-R and MAT2016-76595-R is gratefully acknowledged. We also acknowledge partial funding by Plan de Ciencia, Tecnología e Innovación 2013-2017 del Principado de Asturias and FEDER through grant GRUPIN14-056. M.A-V.is thankful to MINECO and for his pre-doctoral contract. R.R.R acknowledges financial support from MINECO through “Juan de la Cierva” program (JCI-2012-12664).

References

- [1] H. Huang, X. Wang, Recent progress on carbon-based support materials for electrocatalysts of direct methanol fuel cells, *J. Mater.Chem. A* 2 (2014) 6266.
- [2] M. Liu, R. Zhang, W. Chen, Graphene-supported nanoelectrocatalysts for fuel cells: Synthesis, properties, and applications, *Chem. Rev.* 114 (2014) 5117.
- [3] X. Zhao, M. Yin, L. Ma, L. Liang, C. Liu, J. Liao, T. Lu, W. Xing, Recent advances in catalysts for direct methanol fuel cells, *Energy Environ. Sci.* 4 (2011) 2736.
- [4] S.K. Kamarudina, F. Achmada, W.R.W. Dauda, Overview on the application of direct methanol fuel cell (DMFC) for portable electronic devices, *Int. J. Hydrog. Energy* 34 (2009) 6902.
- [5] A. Heinzela, V.M. Barragán, A review of the state-of-the-art of the methanol crossover in direct methanol fuel cells, *J.Power Sources* 84 (1999) 70.
- [6] S.Lj. Gojkovića, T.R. Vidakovića, D.R. Đurovićb, Kinetic study of methanol oxidation on carbon-supported PtRu electrocatalyst, *Electrochim. Acta* 48 (2003) 3607.
- [7] H. Liu, C. Song, L. Zhang, J. Zhang, H. Wang, D.P. Wilkinson, A review of anode catalysis in the direct methanol fuel cell, *J. Power Sources* 155 (2006) 95.
- [8] S.J. Peighambardoust, S. Rowshanzamir, M. Amjadi, Review of the proton exchange membranes for fuel cell applications, *Int. J. Hydrog. Ener.* 35 (2010) 9349.
- [9] J.R.Varcoe, R.C.T. Slade, Prospects for alkaline anion-exchange membranes in low temperature fuel cells, *Fuel Cells* 5 (2005) 187.
- [10] E. Antolini, T. Lopes, E.R. Gonzalez, An overview of platinum-based catalysts as methanol-resistant oxygen reduction materials for direct methanol fuel cells, *J. Alloys Compd.* 461 (2008) 253.
- [11] C. Lamy, A. Lima, V. LeRhun, F. Delime, C. Coutanceau, J.-M. Léger, Recent advances in the development of direct alcohol fuel cells (DAFC), *J. Power Sources* 105 (2002) 283.
- [12] Y. Mu, H. Liang, J. Hu, L. Jiang, L. Wan, Controllable Pt nanoparticle deposition on carbon nanotubes as an anode catalyst for direct methanol fuel cells, *J. Phys. Chem. B* 109 (2005) 22212.
- [13] X. Wang, W. Wang, Z. Qi, C. Zhao, H. Ji, Z. Zhang, High catalytic activity of ultrafine nanoporous palladium for electro-oxidation of methanol, ethanol, and formic acid, *Electrochem. Commun.* 11 (2009) 1896.

- [14] M.A.A. Rahim, R.M.A. Hameed, M.W. Khalil, Nickel as a catalyst for the electro-oxidation of methanol in alkaline medium, *J. Power Sources* 134 (2004) 160.
- [15] G. Karim-Nezhad, P.S. Dorraji, Copper chloride modified copper electrode: Application to electrocatalytic oxidation of methanol, *Electrochim. Acta* 55 (2010) 3414.
- [16] M. Jafarian, M.G. Mahjani, H. Heli, F. Gobal, H. Khajehsharifi, M.H. Hamed, A study of the electro-catalytic oxidation of methanol on a cobalt hydroxide modified glassy carbon electrode, *Electrochim. Acta* 48 (2003) 3423.
- [17] G. Che, B.B. Lakshmi, E.R. Fisher, C.R. Martin, Carbon nanotubule membranes for electrochemical energy storage and production, *Nature* 393 (1998) 346.
- [18] Z. Liu, X.Y. Ling, X. Su, J.Y. Lee, Carbon-supported Pt and PtRu nanoparticles as catalysts for a direct methanol fuel cell, *J. Phys. Chem. B* 108 (2004) 8234.
- [19] F. Su, J. Zeng, X. Bao, Y. Yu, J.Y. Lee, X.S. Zhao, Preparation and characterization of highly ordered graphitic mesoporous carbon as a Pt catalyst support for direct methanol fuel cells, *Chem. Mater.* 17 (2005) 3960.
- [20] C.A. Bessel, K. Laubernds, N.M. Rodriguez, R.T.K. Baker, Graphite nanofibers as an electrode for fuel cell applications, *J. Phys. Chem. B* 105 (2001) 1115.
- [21] C. Xu, X. Wang, J. Zhu, Graphene - Metal particle nanocomposites, *J. Phys. Chem. C*, 112 (2008) 19841.
- [22] K.S. Novoselov, A.K. Geim, S.V. Morozov, D. Jiang, Y. Zhang, S.V. Dubonos, I.V. Grigorieva, A.A. Firsov, Electric Field Effect in Atomically Thin Carbon Films, *Science* 306 (2004) 666.
- [23] A.K. Geim, K.S. Novoselov, The Rise of Graphene, *Nat. Mater.* 6 (2007) 183.
- [24] X. Zhou, X. Huang, X. Qi, S. Wu, C. Xue, F.Y.C. Boey, Q. Yan, P. Chen, H. Zhang, In situ synthesis of metal nanoparticles on single-layer graphene oxide and reduced graphene oxide surfaces, *J. Phys. Chem. C* 113 (2009) 10842.
- [25] X. Chen, G. Wu, J. Chen, X. Chen, Z. Xie, X. Wang, Synthesis of "clean" and well-dispersive Pd nanoparticles with excellent electrocatalytic property on graphene oxide, *J. Am. Chem. Soc.* 133 (2011) 3693.
- [26] I.V. Lightcap, T.H. Kosel, P.V. Kamat, Anchoring semiconductor and metal nanoparticles on a two-dimensional catalyst mat storing and shuttling electrons with reduced graphene oxide, *Nano Lett.* 10 (2010) 577.
- [27] Y. Shao, S. Zhang, C. Wang, Z. Nie, J. Liu, Y. Wang, Y. Lin, Highly durable graphene nanoplatelets supported Pt nanocatalysts for oxygen reduction, *J. Power Sources*. 195 (2010) 4600.

- [28] Y. Shen, M.Z. Zhang, K. Xiao, J. Xi, Synthesis of Pt, PtRh, and PtRhNi alloys supported by pristine graphene nanosheets for ethanol electrooxidation, *ChemCatChem*, 6 (2014) 3254.
- [29] J. Zhao, H. Li, Z. Liu, W. Hu, C. Zhao, D. Shi, An advanced electrocatalyst with exceptional electrocatalytic activity via ultrafine Pt-based trimetallic nanoparticles on pristine graphene, *Carbon* 87 (2015) 116.
- [30] J. Zhao, Z. Liu, H. Li, W. Hu, C. Zhao, P. Zhao, D. Shi, Development of a highly active electrocatalyst via ultrafine Pd nanoparticles dispersed on pristine graphene, *Langmuir* 31 (2015) 2576.
- [31] Y. Shen, Z. Zhang, K. Xiao, J. Xi, Electrocatalytic activity of Pt subnano/nanoclusters stabilized by pristine graphene nanosheets, *Phys. Chem. Chem. Phys.* 16 (2014) 21609.
- [32] Y. Shen, Z. Zhang, R. Long, K. Xiao, J. Xi, Synthesis of ultrafine Pt nanoparticles stabilized by pristine graphene nanosheets for electro-oxidation of methanol, *ACS Appl. Mater. Interfaces* 6 (2014) 15162.
- [33] Y. Shen, K. Xiao, J. Xi, X. Qiu, Comparison study of few-layered graphene supported platinum and platinum alloys for methanol and ethanol electro-oxidation, *J. Power Sources* 278 (2015) 235.
- [34] M. Ayán-Varela, J.I. Paredes, L. Guardia, S. Villar-Rodil, J.M. Munuera, M. Díaz-González, C. Fernández-Sánchez, A. Martínez-Alonso, J.M.D. Tascón, Achieving extremely concentrated aqueous dispersions of graphene flakes and catalytically efficient graphene-metal nanoparticle hybrids with flavin mononucleotide as a high-performance stabilizer, *ACS Appl. Mater. Interfaces* 7 (2015) 10293.
- [35] M. Sevilla, C. Sanchís, T. Valdés-Solís, E. Morallón, A.B. Fuertes, Highly dispersed platinum nanoparticles on carbon nanocoils and their electrocatalytic performance for fuel cell reactions, *Electrochim. Acta* 54 (2009) 2234.
- [36] S. Domínguez-Domínguez, J. Arias-Pardilla, A. Berenguer-Murcia, E. Morallón, D. Cazorla-Amorós, Electrochemical deposition of platinum nanoparticles on different carbon supports and conducting polymers, *J. Appl. Electrochem.* 38 (2008) 259.
- [37] K.R. Paton, E. Varrla, C. Backes, R.J. Smith, U. Khan, A. O'Neil, C. Boland, M. Lotya, O.M. Istrate, P. King, T. Higgins, S. Barwich, P. May, P. Puczkarski, I. Ahmed, M. Moebius, H. Pettersson, E. Long, J. Coelho, S.E. O'Brien, E.K. McGuire, B. Mendoza Sanchez, G.S. Duesberg, N. McEvoy, T.J. Pennycook, C. Downing, A. Crossley, V. Nicolosi, J.N. Coleman, Scalable Production of Large Quantities of

- Defect-Free Few-Layer Graphene by Shear Exfoliation in Liquids, *Nature Mater.* 13 (2014) 624.
- [38] L.M. Malard, M.A. Pimenta, G. Dresselhaus, M.S. Dresselhaus, Raman Spectroscopy in Graphene, *Phys. Rep.* 472 (2009) 51.
- [39] A.C. Ferrari, D.M. Basko, Raman Spectroscopy as a Versatile Tool for Studying the Properties of Graphene, *Nat. Nanotechnol.* 8 (2013) 235.
- [40] L. Guardia, M.J. Fernández-Merino, J.I. Paredes, P. Solís-Fernández, S. Villar-Rodil, A. Martínez-Alonso, J.M.D. Tascón, High-Throughput Production of Pristine Graphene in an Aqueous Dispersion Assisted by Non-Ionic Surfactants, *Carbon* 49 (2011) 1653.
- [41] Z. Sun, J. Masa, Z. Liu, W. Schuhmann, M. Muhler, Highly Concentrated Aqueous Dispersions of Graphene Exfoliated by Sodium Taurodeoxycholate: Dispersion Behavior and Potential Application as a Catalyst Support for the Oxygen-Reduction Reaction, *Chem. Eur. J.* 18 (2012) 6972.
- [42] L. Zhang, Z. Zhang, C. He, L. Dai, J. Liu, L. Wang, Rationally Designed Surfactants for Few-Layered Graphene Exfoliation: Ionic Groups Attached to Electron Deficient π -Conjugated Unit through Alkyl Spacers, *ACS Nano* 8 (2014) 6663.
- [43] M. Buzaglo, M. Shtein, S. Kober, R. Lovrinčić, A. Vilan, O. Regev, Critical Parameters in Exfoliating Graphite into Graphene, *Phys. Chem. Chem. Phys.* 15 (2013) 4428.
- [44] A.B. Bourlinos, V. Georgakilas, R. Zboril, T.A. Steriotis, A.K. Stubos, C. Trapalis, Aqueous-Phase Exfoliation of Graphite in the Presence of Polyvinylpyrrolidone for the Production of Water-Soluble Graphenes, *Solid State Commun.* 149 (2009) 2172.
- [45] S.M. Notley, Highly Concentrated Suspensions of Graphene through Ultrasonic Exfoliation with Continuous Surfactant Addition, *Langmuir* 28 (2012) 14110.
- [46] J.-W.T. Seo, A.A. Green, A.L. Antaris, M.C. Hersam, High Concentration Aqueous Dispersions of Graphene using Nonionic Biocompatible Block Copolymers, *J. Phys. Chem. Lett.* 2 (2011) 1004.
- [47] D. Parviz, S. Das, H.S.T. Ahmend, F. Irin, S. Bhattacharia, M.J. Green, Dispersions of Non-Covalently Functionalized Graphene with Minimal Stabilizer, *ACS Nano* 6 (2012) 8857.
- [48] A. Bonanni, M. Pumera, Surfactants used for dispersion of graphenes exhibit strong influence on electrochemical impedance spectroscopic response, *Electrochem. Commun.* 16 (2012) 19.

- [49] D.A.C. Brownson, C.E. Banks, Fabricating graphene supercapacitors: Highlighting the impact of surfactants and moieties, *Chem. Commun.* 48 (2012) 1425.
- [50] D.A.C. Brownson, C.E. Banks, Graphene electrochemistry: Surfactants inherent to graphene inhibit metal analysis, *Electrochem. Commun.* 13 (2011) 111.
- [51] S. Wang, L. Kuai, Y. Huang, X. Yu, Y. Liu, W. Li, L. Chen, B. Geng, A Highly efficient, clean-surface, porous platinum electrocatalyst and the inhibition effect of surfactants on catalytic activity, *Chem. Eur. J.* 19 (2013) 240.
- [52] Y.M. Li, L.H. Tang, J.H. Li, Preparation and electrochemical performance for methanol oxidation of Pt/graphene nanocomposites, *Electrochem. Commun.* 11 (2009) 846.
- [53] Q. Liang, L. Zhang, M. Cai, Y. Li, K. Jiang, X. Zhang, P.K. Shen, Preparation and characterization of Pt/functionalized graphene and its electrocatalysis for methanol oxidation, *Electrochim. Acta* 111 (2013) 275.
- [54] T.H.T. Vu, T.T.T. Tran, H.N.T. Le, L.T. Tran, P.H.T. Nguyen, H.T. Nguyen, N.Q. Bui, Solvothermal synthesis of Pt-SiO₂/graphene nanocomposites as efficient electrocatalyst for methanol oxidation, *Electrochim. Acta* 161 (2015) 335.
- [55] X. Li, Y. Zhao, H. Wang, H. Tang, J. Tian, Y. Fan, Highly dispersed Pd nanoparticles on 9-amino-1-azabenzanthrone functionalized graphene-like carbon surface for methanol electrooxidation in alkaline medium, *Mater. Chem. Phys.* 144 (2014) 107.
- [56] Y. Zhao, L. Zhan, J. Tian, S. Nie, Z. Ning, Enhanced electrocatalytic oxidation of methanol on Pd/polypyrrole-graphene in alkaline medium, *Electrochim. Acta* 56 (2011) 1967.
- [57] H. Li, G. Chang, Y. Zhang, J. Tian, S. Liu, Y. Luo, A.M. Asiri, A.O. Al-Youbi, X. Sun, Photocatalytic synthesis of highly dispersed Pd nanoparticles on reduced graphene oxide and their application in methanol electro-oxidation, *Catal. Sci. Technol.* 2 (2012) 1153.
- [58] P. Zhong, Y.J. Fan, H. Wang, R.X. Wang, L.L. Fan, X.C. Shen, Z.J. Shi, Copper phthalocyanine functionalization of graphene nanosheets as support for platinum nanoparticles and their enhanced performance toward methanol oxidation, *J. Power Sources* 242 (2013) 208.
- [59] Y. Li, W. Gao, L. Ci, C. Wang, P.M. Ajayan. Catalytic performance of Pt nanoparticles on reduced graphene oxide for methanol electro-oxidation. *Carbon* 48 (2010) 1124.

- [60] S. Lin, C. Shen, D. Lu, C. Wang, H-J. Gao. Synthesis of Pt nanoparticles anchored on graphene encapsulated Fe₃O₄ magnetic nanospheres and their use as catalysts for methanol oxidation. *Carbon* 53 (2013) 112.
- [61] X. Chen, Z. Cai, M. Oyama, X. Chen. Synthesis of bimetallic PtPd nanocubes on graphene with N,N-dimethylformamide and their direct use for methanol electrocatalytic oxidation. *Carbon* 66 (2014) 112.
- [62] S. Sharma, B.G. Pollet, Support materials for PEMFC and DMFC electrocatalysts - A review, *J. Power Sources* 208 (2012) 96.
- [63] J. Duan, X. Zhang, W. Yuan, H. Chen, S. Jiang, X. Liu, Y. Zhang, L. Chang, Z. Sun, J. Du, Graphene oxide aerogel-supported Pt electrocatalysts for methanol oxidation, *J. Power Sources* 285 (2015) 76.
- [64] Z. Wang, G. Shi, F. Zhang, J. Xia, R. Gui, M. Yang, S. Bi, L. Xia, Y. Li, L. Xia, Y. Xia, Amphoteric surfactant promoted three-dimensional assembly of graphene micro/nanoclusters to accommodate Pt nanoparticles for methanol oxidation, *Electrochim. Acta* 160 (2015) 288.
- [65] J.S. Spendelow, A. Wieckowski, Electrocatalysis of oxygen reduction and small alcohol oxidation in alkaline media, *Phys. Chem. Chem. Phys.* 9 (2007) 2654.
- [66] K. Matsuoka, Y. Iriyama, T. Abe, M. Matsuoka, Z. Ogumi, Alkaline direct alcohol fuel cells using an anion exchange membrane, *J. Power Sources* 150 (2005) 27.
- [67] A. Chen, C. Ostrom, Palladium-Based Nanomaterials: Synthesis and Electrochemical Applications, *Chem. Rev.* 115 (2015) 11999.

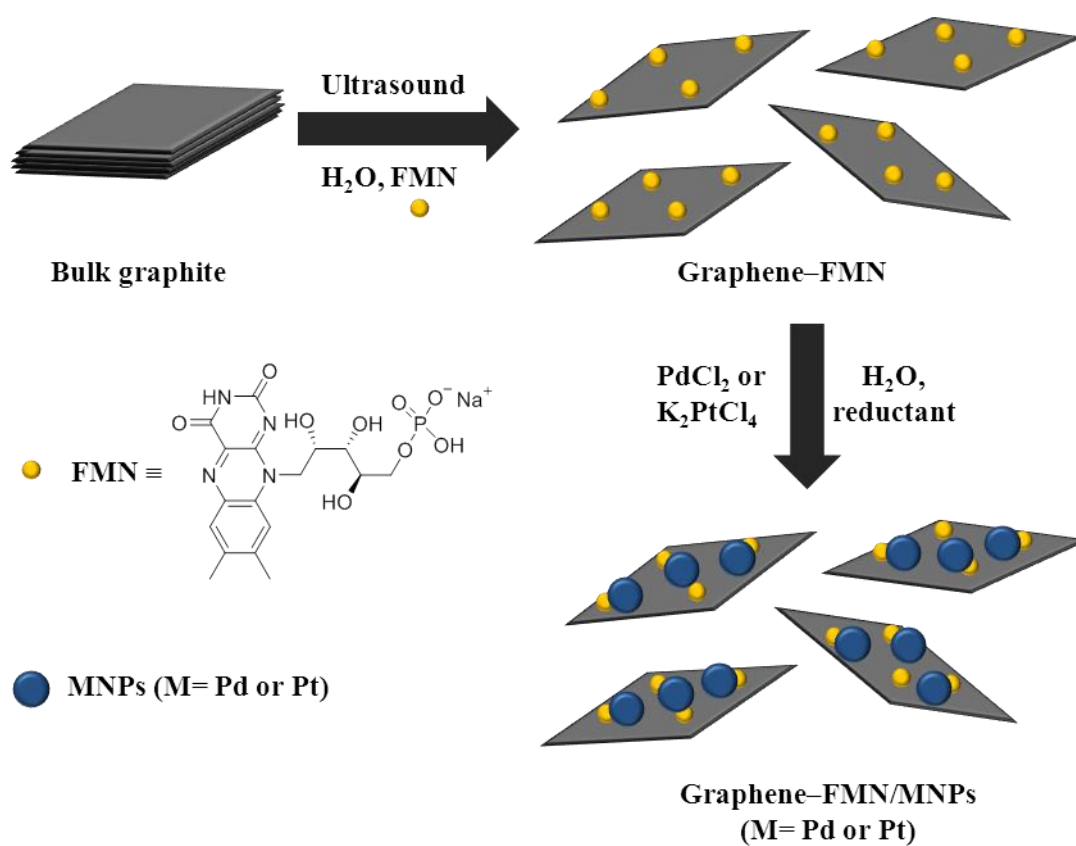


Figure 1. Schematic of the FMN-assisted exfoliation and stabilization in water of pristine graphene, followed by the preparation of pristine graphene-metal NP hybrids.

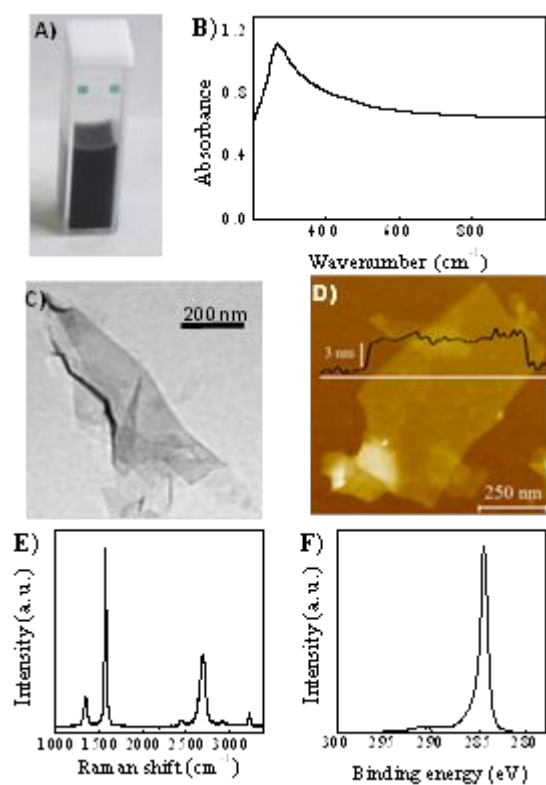


Figure 2. (A) Digital photograph and (B) typical UV–vis absorption spectrum of FMN-exfoliated graphene colloidal dispersion in water. (C) Representative TEM image of an exfoliated graphene flake. (D) AFM image of a graphene flake deposited onto a SiO₂/Si substrate. A typical line profile (black trace) taken along the marked white line is shown overlaid on the image. (E) Raman and (F) high resolution C1s XPS spectra of the same material.

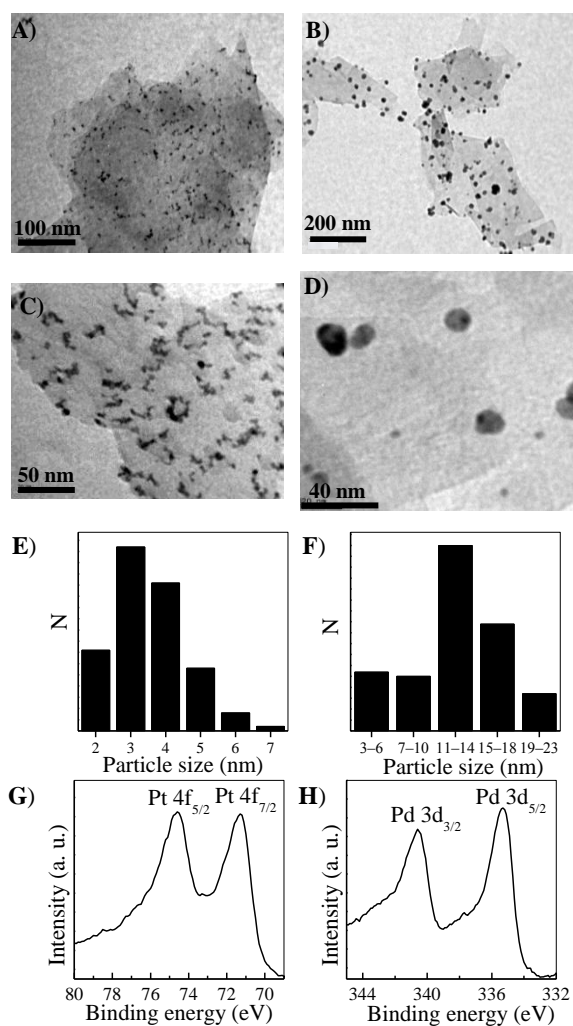


Figure 3. The left column shows results from the characterization of graphene-Pt NP hybrid (A,C,E,G), while the right column shows results for the graphene-Pd NP(1) hybrid (B,D,F,H). Specifically: representative TEM images (A–D); NP size distribution estimated from the TEM images (E,F); high resolution core level XPS spectrum of (G) Pt 4f and (H) Pd 3d.

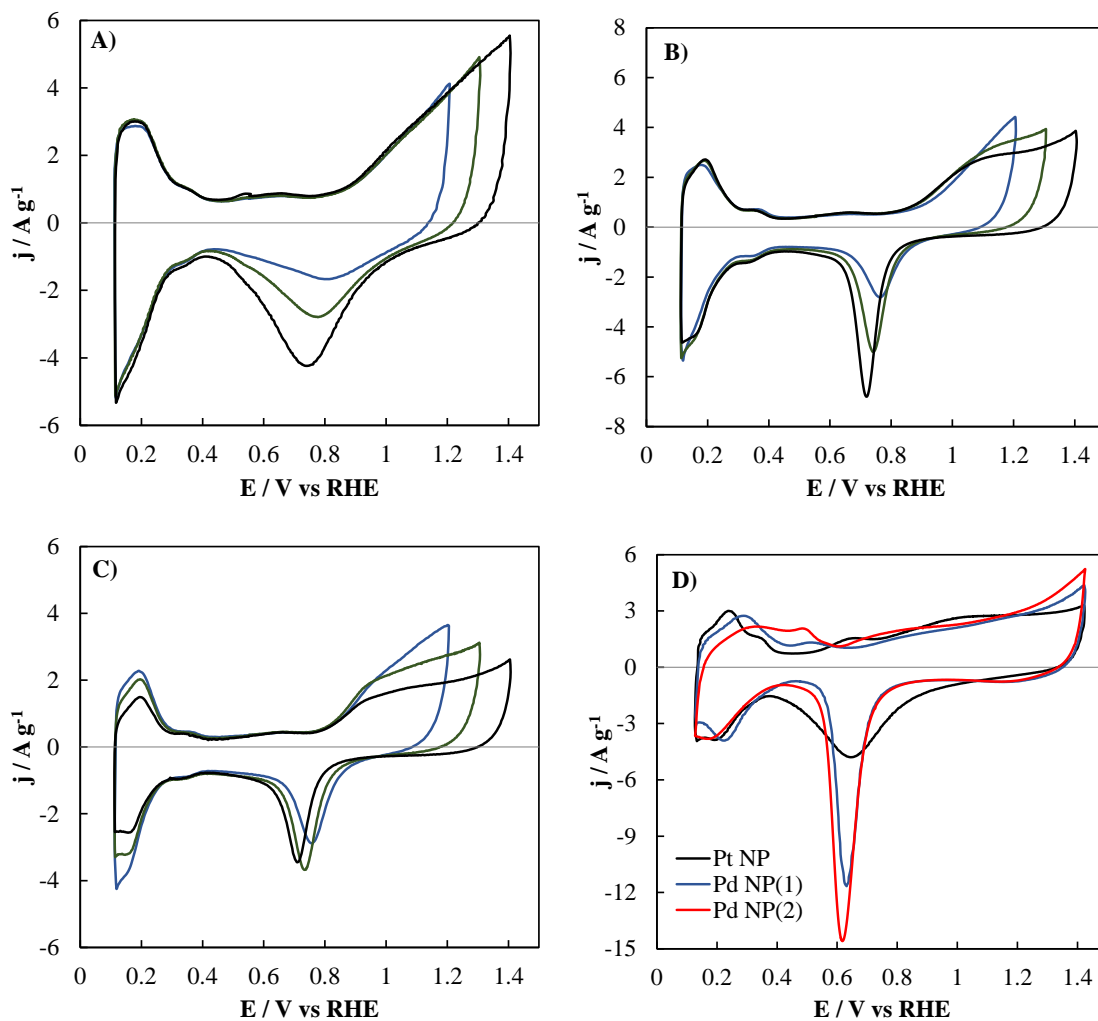


Figure 4. (A–C) Cyclic voltammograms (5th scan) of all the hybrids prepared in this work in 0.5 M H₂SO₄ solution at 50 mV s⁻¹: (A) graphene–Pt NP hybrid (B), graphene–Pd NP(1) hybrid, and (C) graphene–Pd NP(2) hybrid. The upper potential limit was step-wise opened from 1.2 to 1.4 V after recording five CV scans. (D) Cyclic voltammograms of all the hybrids prepared in this work in 0.1 M KOH solution at 50 mV s⁻¹.

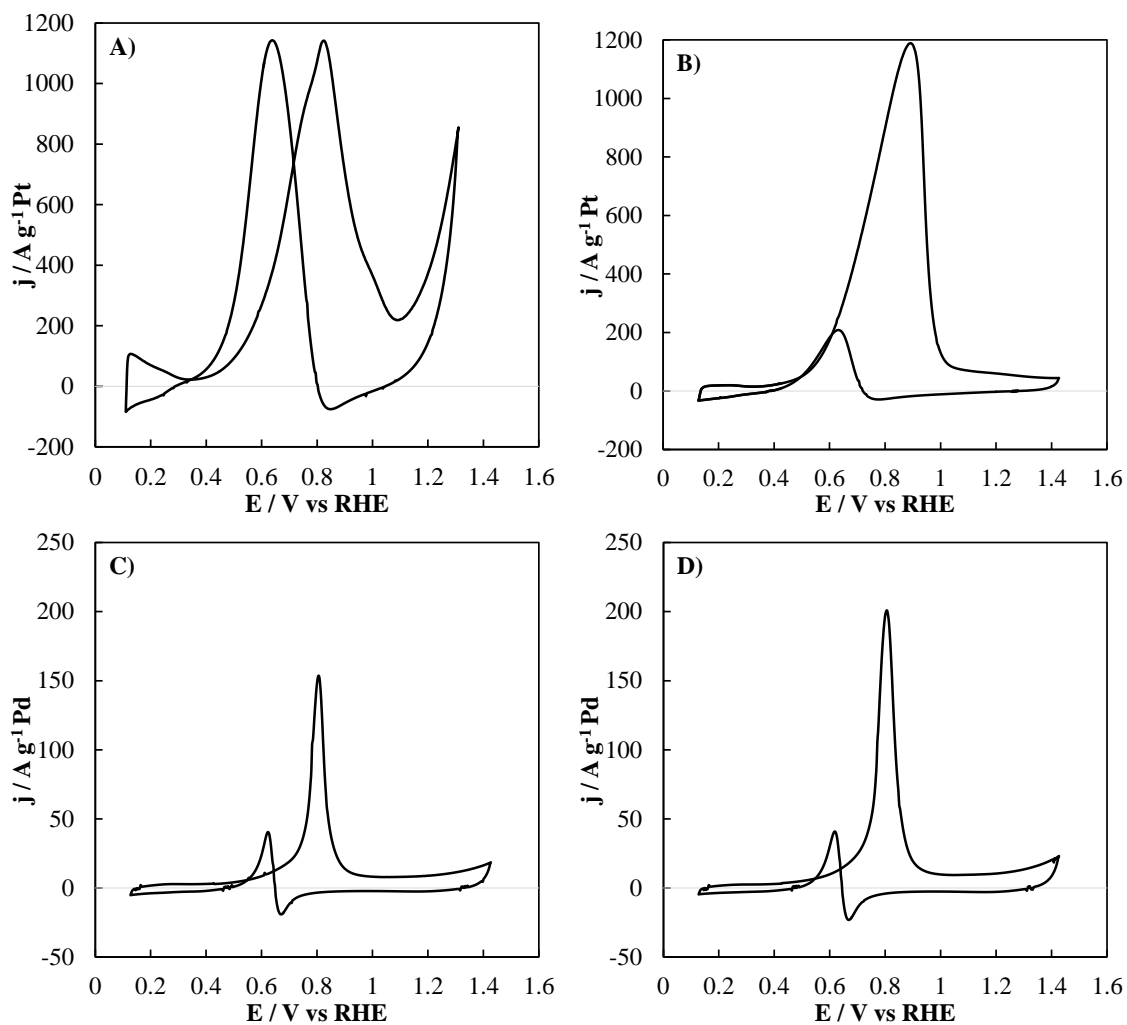


Figure 5. Steady state cyclic voltammograms obtained at 10 mV s^{-1} and in the presence of 0.5 M MeOH in the solution for the graphene-Pt NP hybrid in (A) 0.5 M H_2SO_4 and (B) 0.1 M KOH and for the (C) the graphene-Pd NP(1) and (D) the graphene-Pd NP(2) hybrid electrodes in 0.1 M KOH.

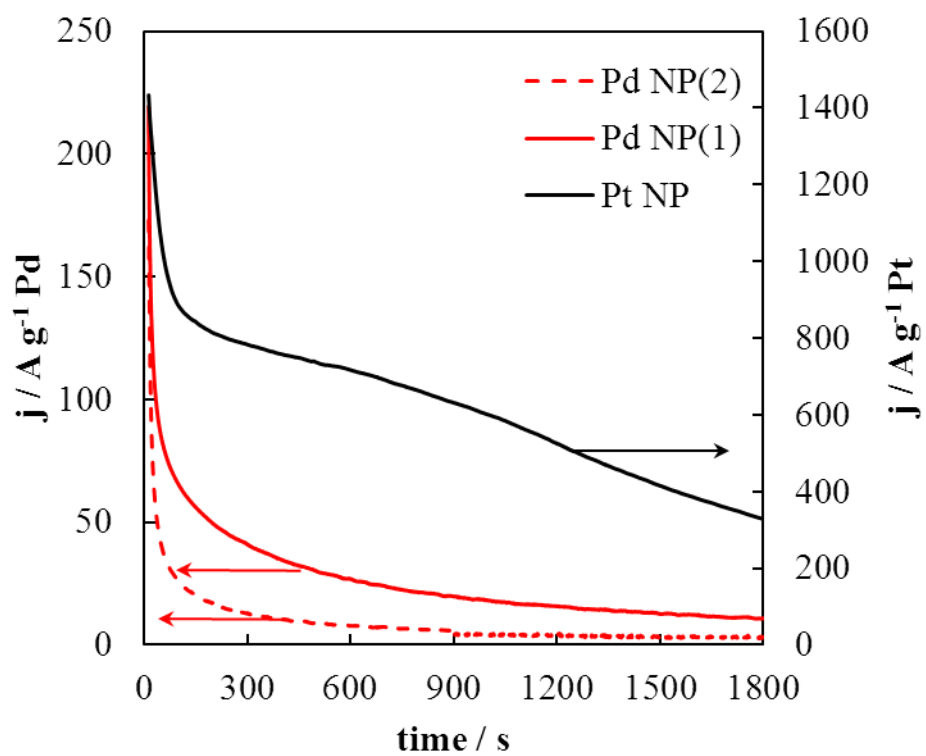


Figure 6. Current-time profiles measured by chronoamperometry at 0.80 V in 0.1 M KOH + 1 M MeOH for the graphene–Pt NP and –Pd NP hybrids.

Table 1. Electrocatalytic activity for MOR of graphene and RGO–metal NP hybrids and comparison with other relevant works on the catalytic activity for methanol oxidation.

Sample	ECSA	GSA	j_F^{KOH}	I_F/I_B^{KOH}	$j_F^{\text{H}_2\text{SO}_4}$	$I_F/I_B^{\text{H}_2\text{SO}_4}$	Ref.	
	$\text{m}^2 \text{g}^{-1}$	$\text{m}^2 \text{g}^{-1}$	A g^{-1}		A g^{-1}			
graphene–Pt hybrid	NP	49.2	62	1180	4.03	1140	1.00	This work
graphene–Pd hybrid	NP(1)	24.6	37	154	3.81	low	--	This work
graphene–Pd hybrid	NP(2)	26.3	66	248	4.92	low	--	This work
FLG–Pt		62.9				410		[33]
GNS–ultrafine Pt		91				400	0.85	[32]
GNS–Pt nanoclusters		112				209		[31]
PG–ultrafine Pd		115		1045.7		823.4		[30]
RGO–ultrafine Pd		53.9		526.1		447.3		[30]
Pt/GO aerogel & Pt/RGO						876/192		[63]
RGO–Pt nanocomposite		44.6				199.6		[53]
copper phtalocyanine RGO–Pt		42.9				730.3		[58]
PyS/RGO–Pt nanocomposites		48.6				279.5	1.37	[53]
SiO ₂ /RGO–Pt		87.2				1047	1.04	[54]
(arc discharge)GN–Pt/3D		108.6				1167.3	1.57	[64]
amino-azabenzanthrone		19.0		770				[55]

RGO–Pd					
Polypyrrole RGO–Pd	41.8	359.8	7.3		[56]
		(NaOH)			
Photocatalytic RGO–Pd	13.3			A cm ⁻²	[57]
				units	
PtNPs/RGO	36.27			A cm ⁻² 0.83	[59]
				units	
PtNPs/RGO	33.55			130 0.84	[60]
PtPdNanocubes/RGO	45.1			520 1.27	[61]
